Bone Reports 14 (2021) 101064

Contents lists available at ScienceDirect

Bone Reports

journal homepage: www.elsevier.com/locate/bonr

The application of Bonelike® Poro as a synthetic bone substitute for the management of critical-sized bone defects - A comparative approach to the autograft technique - A preliminary study

P.O. Pinto [a,b,c,1], M.V. Branquinho [a,b,1], A.R. Caseiro [b,c], A.C. Sousa [a,b], A. Brandão [g], S. S. Pedrosa [b], R.D. Alvites [a,b], J.M. Campos [b,c], F.L. Santos [a,b], J.D. Santos [f], C.M. Mendonça [a,b], I. Amorim [d,e], L.M. Atayde [a,b], A.C. Maurício [a,b,*]

[a] Veterinary Clinics Department, Abel Salazar Biomedical Sciences Institute (ICBAS), University of Porto (UP), Rua de Jorge Viterbo Ferreira, nº 228, 4050-313, Porto, Portugal

[b] Animal Science Studies Centre (CECA), Agroenvironment, Technologies and Sciences Institute (ICETA), University of Porto, Rua D. Manuel II, Apartado 55142, 4051-401 Porto, Portugal

[c] Vasco da Gama Research Center (CIVG), Vasco da Gama University School (EUVG), Av. José R. Sousa Fernandes 197, Campus Universitário, Lordemão, 3020-210 Coimbra, Portugal

[d] Department of Pathology and Molecular Immunology, Abel Salazar Institute of Biomedical Sciences (ICBAS), University of Porto (UP), Rua Jorge Viterbo Ferreira, n º 228, 4050-313 Porto, Portugal

[e] Institute of Research and Innovation in Health (i3S), University of Porto (UP), Rua Alfredo Allen, 4200-135 Porto, Portugal

[f] Network of Chemistry and Technology – Associated Laboratory for Green Chemistry (REQUIMTE-LAQV), Department of Metallurgy and Materials, Faculty of Engineering, University of Porto, Rua Dr Roberto Frias s/n, 4200-465 Porto, Portugal

[g] Biosckin, Molecular and Cell Therapies, SA, Parque de Ciência e Tecnologia da Maia, Rua Eng. Frederico Ulrich, 2650, 4470-605 Moreira da Maia, Portugal

ARTICLE INFO

Keywords:
Bone regeneration
Critical bone defects
Ceramic biomaterials
Bonelike®
Ovine model

ABSTRACT

The effective treatment of non-unions and critical-sized defects remains a challenge in the orthopedic field. From a tissue engineering perspective, this issue can be addressed through the application bioactive matrixes to support bone regeneration, such as Bonelike®, as opposed to the widespread autologous grafting technique. An improved formulation of Bonelike® Poro, was assessed as a synthetic bone substitute in an ovine model for critical-sized bone defects. Bone regeneration was assessed after 5 months of recovery through macro and microscopic analysis of the healing features of the defect sites. Both the application of natural bone graft or Bonelike® Poro resulted in bridging of the defects margins. Untreated defect remained as fibrous non-unions at the end of the study period. The characteristics of the newly formed bone and its integration with the host tissue were assessed through histomorphometric and histological analysis, which demonstrated Bonelike® Poro to result in improved healing of the defects. The group treated with synthetic biomaterial presented bone bridges of increased thickness and bone features that more closely resembled the native spongeous and cortical bone. The application of Bonelike® Poro enabled the regeneration of critical-sized lesions and performed comparably to the autograph technique, validating its octeoconductive and osteointegrative potential for clinical application as a therapeutic strategy in human and veterinary orthopedics.

1. Introduction

Under normal biological situations, a skeletal fracture will resolve spontaneously within the first six to eight weeks after the injury. When biological or mechanical disturbances occur in the regenerative environment or when the fracture has occurred in thick cortices bones (such as the femoral or tibial diaphysis), the regenerative process becomes challenging and increased time is required for fracture healing.

Such clinical situations benefit from strategies to promote and enhance the healing process, in order to restore the original bone

* Corresponding author at: Veterinary Clinics Department, Abel Salazar Biomedical Sciences Institute (ICBAS), University of Porto (UP), Rua de Jorge Viterbo Ferreira, nº 228, 4050-313, Porto, Portugal.
E-mail address: acmauricio@icbas.up.pt (A.C. Maurício).

[1] P.O. Pinto and M.V. Branquinho contributed equally and should both be considered as first authors.

https://doi.org/10.1016/j.bonr.2021.101064
Received 13 January 2021; Received in revised form 16 March 2021; Accepted 5 April 2021
Available online 9 April 2021

structure and function. These scenarios are observed in both human and veterinary medicine (Calori et al., 2011; Vertenten et al., 2010), and include traumatic injuries or tumor resections (with substantial and irregular bone loss), gaps resulting from open wedges corrective osteotomies, arthrodesis or arthroplasties, spinal fusion, non-union or delayed bone unions, metabolic diseases, and other local or systemic diseases, all often related to aged patients. In these scenarios, bone regeneration is compromised, and the bone defect exceeds the intrinsic biological restoration mechanisms capacity (Calori et al., 2011; Vertenten et al., 2010; Gutierres et al., 2007; Innes, 2014).

The critical-sized bone defects (CSBD) are the smallest bone defect that will not heal spontaneously without a specific treatment during lifetime of the individual (Hollinger and Kleinschmidt, 1990). The effective volume and size of such defects is dependent on the bone and animal species (Gosain et al., 2000), and therefore their definition is not consensually described (Schemitsch, 2017). Critical-sized defects usually present stable biological and molecular responses, but major tissue loss impairs bone regeneration.

In parallel, if after four months healing is not observed, the situation is defined as a case of delayed union and, if after six months no bone healing is observed, the clinical classification of a non-union is established (Carlier et al., 2014; Gómez-Barrena et al., 2015; Trejo-Iriarte et al., 2019). Unlike critical-sized defects, a biomechanical impairment is present in non-unions, with damaged molecular and cellular signaling, although a bone gap is not necessarily present (Schemitsch, 2017).

In clinical scenarios, if the bone union does not occur within one year it is unlikely to ever occur, resulting in permanent non-union, with fibrous scar formation between the bone edges, without restoration of bone continuity and function (Hollinger and Kleinschmidt, 1990). Thus, while critical-sized defects are defined as requiring surgical bone grafting, non-unions can eventually heal without applying bone grafting (Schemitsch, 2017). These clinical cases often result in poor outcomes and are a challenging topic for orthopedic surgeons. Different treatment strategies can be used to improve new bone formation, avoiding formation of tissue with inferior quality (Calori et al., 2011; Vertenten et al., 2010; Innes, 2014; Cross et al., 2012; Johnson et al., 2005; Campana et al., 2014).

The healing of these defects can be achieved through appropriate treatment (Roddy et al., 2018), such as autologous cancellous bone grafting (ACBG), currently considered as the gold standard technique. In the last decades, the well-known disadvantages of autografts and allografts have encouraged the development of alternative methods.

Tissue engineering strategies are a promising option for large bone defects treatment and can include an osteoconductive scaffold for matrix support, growth factors to promote osteoinduction and vascularization of the site, and the application of cellular systems with osteogenic potential (Berner et al., 2012). From this perspective, an ideal natural or synthetic bone substitute should be biocompatible, resorbable, with a similar mechanical resistance as the cortical bone, have osteoconductive, osteoinductive and osteogenic properties, and be easily handled and sterilized. Further, the bone substitute should not cause any adverse systemic nor local reaction and must provide a favorable environment to be invaded by blood vessels, cells and growth factors (Campana et al., 2014; Blokhuis et al., 2000).

The limited number of natural bone grafts available has increased the importance of applying synthetic bone grafts as substitutes, and among the most used materials are calcium sulfate, calcium phosphate ceramics and cements, bioactive glasses, poly(methyl methacrylate) or combinations between different materials. The ideal option has not yet been defined (Wang and Yeung, 2017). Calcium sulfate is a biodegradable and osteoconductive ceramic that has been used to fill critical bone defects since the 1980s. Despite having a macroporous structure, the fact that it is absorbed very quickly and has a weak internal strength, its use is more suitable for small bone defects with rigid internal fixation (Wang and Yeung, 2017; Carson and Bostrom, 2007). Calcium phosphate ceramics are composed of calcium hydroxyapatite whose chemical constitution is similar to that of the mineral phase of calcified organic tissues (Zwingenberger et al., 2012). As they are bioabsorbable ceramics with good osteoconductivity, this type of ceramics has been used in multiple clinical studies (Scheer and Adolfsson, 2009). In this type of material, its porous and crystalline structure is one of the factors to be considered in the selection, and the calcium-to-phosphate ratios can affect its absorption rate and mechanical properties. In hydroxyapatite and tricalcium phosphate this ratio is particularly well identified (Wang and Yeung, 2017). The calcium phosphate cements emerged with the aim of expanding the adaptability and moldability of calcium phosphate ceramics, and unlike the latter, they are made up of two components, one of which is an aqueous curing agent. These cements are generally microporous, biocompatible and provide good mechanical support when subjected to low bending strength (Wang and Yeung, 2017; Alkhraisat et al., 2010). Bioactive glasses or bioglasses are synthetic silicate-based ceramics whose constitution, optimized over the years of research, and has made it possible to obtain a stable physical bonding between bioglass and the host's bone. This connection is thought to be related to the formation of a hydroxyapatite coating on the surface of bioglass that absorbs proteins and attracts osteoprogenitor cells (Wang and Yeung, 2017; Välimäki and Aro, 2006). Despite this, the mechanical properties of these glasses tend to be weak and fragile, which makes them more feasible to simpler defects and in combination with other approaches such as growth factors (Marão et al., 2015). Finally, poly (methyl methacrylate) is a non-biodegradable and non-resorbable bone cement that is commonly used clinically as a synthetic material, although it cannot be considered a true material substitute (Hernández et al., 2009). Despite its widespread use in total joint replacement for the fixation of components, it also has some drawbacks related to its polymerization, mechanical mismatch and inherent inert properties (Wang and Yeung, 2017).

Bonelike® is a glass-reinforced hydroxyapatite (HA) composite [P2O5-CaO glass-based system within a HA matrix] with osteoconductive proprieties that can be applied as a synthetic bone graft. Its advantages have been demonstrated in several clinical applications, namely dental, maxillofacial and orthopedic surgery (Gutierres et al., 2007; Gutierres et al., 2006; Gutierres et al., 2005; Pavan Kumar et al., 2014; Torres et al., 2014). One of the main morphological properties of biomaterials, with the purpose of bone ingrowth, is the existence of open and interconnected pores. According to the literature, these biomaterials must have pores with diameters larger than 100 μm in order to allow a necessary cell migration, vascularisation, metabolic waste removal, and circulation of water and nutrients (Silva et al., 2003; Laranjeira et al., 2009). In order to produce a formulation with this property, new interconnected macroporous 3D structures were developed. Bonelike® Poro (BLP) is a *novel* formulation of polygonal granules with 2000–5600 μm of diameter with pore size range from 200 to 600 μm.

This range of granules size allows the complete filling of the bone defect area, establishing close contact with host bone, thus enhancing new tissue formation through osteoconduction. The macroporosity is generated by adding polyvinyl alcohol and microcrystalline cellulose in HA and bioglass as pore forming agents before sintering, granting the desired pore size and pore interconnectivity. These macroporous structures enhance the surface area of the BLP and allow for cell migration though its porous structure, increasing cell adhesion and proliferation. Furthermore, the pore size ranging from 200 to 600 μm closely resembles that of the trabecular bone, allowing bone ingrowth through the biomaterial structure (Gutierres et al., 2008).

The aim of this study was to evaluate the effectiveness of BLP in promoting bone regeneration as a bioactive matrix and as a synthetic bone substitute in critical-sized bone defects in comparison to autologous grafting techniques, considering an undemanding biomechanical defect. To analyze the osteoconductive potential of BLP and evaluate its efficacy and potential for further clinical use in humans and veterinary orthopedics (Lansdowne et al., 2014), the behavior of BLP bone graft was assessed against positive and negative controls (ACBG and

untreated defects, respectively). The ovine model of iliac crest CSBD was selected for the purpose due to its histologic similarity to human bone, reduced morbidity, relatively low risk of complications, ease of reproduction and the possibility to create two defects per animal that allows the reduction of the number of animals used.

2. Materials and methods

2.1. Bonelike® Poro preparation

The BLP was prepared as briefly detailed: HA and P_2O_5-CaO based glass were individually prepared and mixed. BLP was obtained by adding 2.5 wt% of the glass powder to HA and both mixed with pore forming agents, microcrystalline cellulose and polyvinyl alcohol. The mixture was dried, sintered at 1300 °C and then milled to the appropriate size of granules. Standard sieving techniques were used to obtain the desired ranges of granules, on from 2000 to 5600 μm of diameter with pore sizes range from 200 to 600 μm.

2.2. Biomaterial characterization

Several techniques were used to characterize the BLP, namely X-ray Diffraction (XRD) for phase identification and quantification, Scanning Electron Microscopy (SEM) for materials morphology evaluation (pore size and interconnectivity) and Energy-Dispersive X-ray spectroscopy (EDS) to detect the elements that were present in the structure of BLP.

2.2.1. X-ray diffraction (XRD)

BLP samples were ground to fine powders and were analysed by a Philips X'Pert X-ray diffractometer, using Kα1 radiation characteristic of cobalt (λ = 178,897 Å). Data were acquired from 4 to 100° (2θ), with step size of 0.025°/s. The identification of the different phases was determined based on the comparison with relative standard values, through the intensity of the peaks.

2.2.2. Scanning electron microscopy (SEM) and energy-dispersive x-ray spectroscopy (EDS)

Scanning electron microscope (SEM) analysis and energy dispersive x-ray spectroscopy (EDS) exam were performed using a high resolution (Schottky) Environmental Scanning Electron Microscope with X-Ray Microanalysis and Electron Backscattered Diffraction analysis: Quanta 400 FEG ESEM / EDAX Genesis X4M, operating in high vacuum mode at an accelerating voltage of 15 kV SEM. Samples were coated with gold/palladium for 120 s and with a 15 mA current. Regarding the samples nature, and whenever necessary, electron backscatter diffraction (EBSD) images were obtained.

2.2.3. Microcomputed tomography analysis

Microcomputed tomography (micro-CT) scans were taken for qualitative evaluation of the new bone formed in bone defects, using the SkyScan1275 micro-CT (RJL Micro & Analytic, Karlsdorf-Neuthard, Deutschlan) which operated with a cone-beam X-ray tube. The photons were detected by a 3Mp (1944 × 1536 pixels) active pixel CMOS flat panel. A 1 mm aluminum filter was used for taking optimized images. For each sample, at least 1500 projections/180 of X-rays (80 kVp, 125 μA, 24,5 μm and scanning time 45 min) were acquired. The volume of interest was defined by a cylindrical contour, diameter was defined by the diameter of the drill hole (13.9 mm) and the height was defined by chosen the same number of slices for every sample (300 slices, 7.35 mm). The evaluation was done twice, first with a threshold of 170 to segment the BLP granules only and secondly with a lower threshold of 85 to segment the new bone and the BLP granules.

2.3. In vivo bone regeneration assessment

Animal testing procedures were performed in accordance with the Directive 2010/63/EU of the European Parliament (transposed to the Portuguese Law as DL 113/2013 and DL 1/2019). ICBAS-UP Animal Welfare Organism of the Ethics Committee and the Portuguese Veterinary Authorities approved all animal procedures. In conformity with the OECD guidelines [Guidance Document on the Recognition, Assessment and Use of Clinical Signs as Humane Endpoint for Experimental Animals Used in Safety Evaluation (2000)], humane end points for animal suffering and distress were followed along animal experimentation, and adequate measures were taken in order to minimize pain and discomfort. Experimental details are reported as recommended by the ARRIVE Guidelines (Percie du Sert et al., 2020).

Ovis aries (merino sheep) were included this study: 11 healthy non-pregnant adult female individuals, with an average weight of ~50 kg and aged between 7 and 8 years. An acclimatization period of two weeks, thorough clinical examinations and 12 h fasting were considered prior to surgery.

2.3.1. Surgical procedure

2.3.1.1. Pre-surgical procedure. Premedication including xylazine (Rompun® 20 mg/ml, Bayer, 0,1 mg/kg) and butorphanol (Dolorex® 10 mg/ml, MSD, 0,05 mg/kg) was administered intramuscularly, allowing sedation and trichotomy of both hind limbs. Iodopovidone at 10% (Betadine®) and 70% ethanol were employed at the surgical field. Intraoperatively, intravenous fluid was provided at maintenance rate (NaCl 0,9% B Braun®) and general anaesthesia was induced with intravenous tiletamine-zolazepam (Zoletil®, 100 mg/ml, Virbac, 3 mg/kg). Monitoring of anaesthesia included cardiorespiratory parameters and bolus of tiletamine-zolazepam whenever required. Loco-regional anaesthesia was performed with lidocaine hydrochloride (Anestesin® 2%, 20 mg/ml, Medinfar-Sorológico) administration using an epidural spinal catheter between L6 and S1.

2.3.1.2. Surgical technique. Surgical technique was based on the procedure described by Lansdowne et al. (Lansdowne et al., 2014): the animal was positioned in sternal recumbence and the hind limbs were pulled cranially. Then, a curved ventro-dorsal skin incision was performed at the cranial region of the iliac crest. Subcutaneous tissue was dissected until periosteum was exposed. The *gluteus medius* muscle was incised, 1 cm above his insertion at the iliac crest and the lateral side of the *ileum ala* was exposed. At the medial side, a fascia incision was performed 5 mm distal and parallel to its insertion at the ileum crest. *Iliocostalis* and *longissimus lumborum* muscles were retracted. The procedure was performed bilaterally. Further, the total thickness circular bone defects with 17 mm diameter were created on the mid portion of the *ileum*, using a custom made trephine drill, with continuous cooling of the surgical area with a saline solution (NaCl 0,9% B Braun®), to prevent thermal damage to the bone edges (Fig. 1).

2.3.1.3. Biomaterial and autograft application. Three different groups were considered for this study: a control group of untreated defects (CT), an autograft-treated group (AG) and a biomaterial-treated group (Bonelike®) (BLP). Considering the AG group, autologous cancellous bone removed from the total thickness circular defect was morselized with use of a Rounger, and subsequently applied to the lesion site as defect filler. In the BLP, macroporous Bonelike® formulation mixed with autologous whole blood served as defect filler. After the random allocation of each defect to a study group and therapeutic approach application, local soft tissue was sutured, and the surgical access closed similarly in all groups.

A total of 11 animals were used and bilaterally defects were considered, resulting in a total of 22 defects ($n = 22$), $n = 4$ for the CT group, $n = 7$ for the AG group and $n = 11$ for the BLP group. Treatments were randomly allocated to the defects. Samples sizes match similar studies reported in literature, weighing the balance harm-benefit

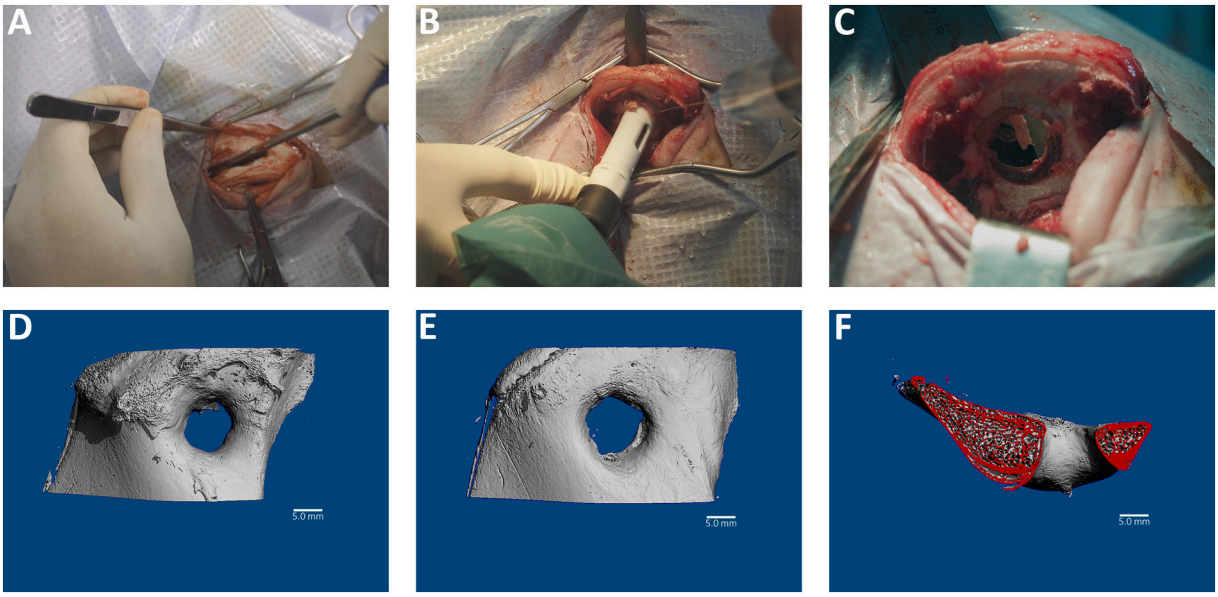

Fig. 1. Sequence of the surgical technique and micro-computed tomography (μCT) imaging of the defect: a) *ileum ala* presenting *gluteus medius* muscle incision; b) total thickness circular bone defects with 17 mm diameter performed on the mid portion of the *ileum*; c) total thickness circular bone defects with 17 mm diameter at the mid portion of the *ileum* before treatment; d), e) and f) μCT imaging of the bone defect area.

analysis (Lansdowne et al., 2014; Atayde et al., 2015; Campos et al., 2018a).

2.3.1.4. Post-surgical procedures. Post-operative radiographs of the defect site were recorded. Positioning the animal in sternal recumbency, a craniomedial to caudolateral oblique view was taken to assess the maintenance of the biomaterials at the site of application and defects location. After complete anaesthetic recovery, animals were transferred to a straw yard, in groups of 4–5 animals and received equal treatment. Prophylactic medication included an antibiotherapy [ampicillin (Albipen LA®, 100 mg/ml, MSD, 20 mg/kg) every 48 h for 6 days] and a non-steroidal anti-inflammatory [meloxicam (Meloxidyl®, 20 mg/ml, Ceva, 0,5 mg/kg) every 48 h for 6 days]. Animals were sacrificed after a recovery period of 5 months. Considering humane conditions and a quiet environment, an overdose of sodium pentobarbital (Euthasol®, 400 mg/ml, Ecuphar, 140 mg/kg) was intravenously administrated after an initial sedation with xylazine and butorphanol, as described above.

Post-mortem, ilea were dissected, and soft tissue removed from the bone. A cranial to caudal tabletop X-ray was obtained for all samples for qualitative evaluation of bone regeneration. Isolated sample sections were individually packed and maintained in 3,7–4% p-formaldehyde (252931.13.15, AppliChem, Panreac®).

Samples were coded and processed blindly for outcome analysis.

2.3.2. Histological processing and scanning electron microscopy (SEM)

Bone sections were further sectioned to obtain samples with the desirable dimensions, containing the defect area, biomaterial and essential surrounding healthy bone tissue.

All the samples were evaluated by X-Ray with a table-top caudal to cranial incidence with 55 Kv and 0.8 mAs.

Samples were further dehydrated in a crescent ethanol concentrations solution series (from 70% to 100%). Briefly, samples were incubated in 70%, 80%, 90%, 96% and 100% ethanol solutions, for 7 days each, shielded from light and under constant agitation. Tissues were then placed in a butanol solution for 7 days, also shielded from light and under constant agitation. Moreover, samples were impregnated with an equal part of absolute ethanol and liquid 2-hydroxyethyl methacrylate solution, for 24 h, again under constant agitation and minimizing light exposure. After the pre-infiltration solution, samples were impregnated in a 2-hydroxyethyl methacrylate resin, for 7 days, under agitation. Samples were consequently placed in the moulds, and soaked in 2-hydroxyethyl methacrylate solution, overnight. After curing, samples were removed from the moulds and were ready to be sectioned. Before sectioning for SEM, samples were sectioned for histological analysis using a diamond blade microtome. The desired section was floated on a water bath and set on a slide. Haematoxylin and Eosin (H&E) staining was performed to each sample. Samples were further sectioned for SEM analysis, using a diamond blades microtome. After sectioning, sample were polished using aluminum oxide disks and diamond spray.

Scanning electron microscope (SEM) analysis and energy dispersive x-ray spectroscopy (EDS) exam were performed as described above.

Complete SEM images of the samples were obtained by stitching, using Image Composite Editor 2.0 software (Microsoft©).

2.3.3. Histomorphometric analysis

Regarding the histomorphometric analysis, SEM images of the defect area were selected with 30× magnification. Unfilled, unmineralized voids, bone and biomaterial fractions were quantified, based on the technique developed by Atayde et al. (2015), Campos et al. (2018a), Atayde et al. (2014). This approach provides an objective and reproducible method for the histomorphometric analysis of the regenerated bone tissue, which is based on the semiautomatic image segmentation (Threshold method) of the histological images, using Image J® software (ImageJ 1.51 k, NIH, USA). Specific content of selected areas of each sample were analysed, according to the pixels frequency in a grey scale. SEM image samples were first converted to 8-bit grey scale format. Using the threshold analysis tool, separation of different grey level, were selected in the pixels histograms, reflecting unmineralized *lacunae*, bone and biomaterial fractions of the sample.

Minimum and maximum threshold values were defined to each fraction analysed and pixel area determined and corrected to the total selection pixel area. To select the unmineralized *voids* pixels (black pixels), the threshold was defined between 0 and 100; for bone pixels fraction (dark grey pixels), the threshold was defined between 101 and 220; and for the unfilled area (connective tissue) fraction (originally black pixels converted to very light grey pixels with Adobe Photoshop CC), the threshold was defined between 221 and 240. Regarding the BL group, bone fraction pixels was defined between 101 and 159, and for

the biomaterial fraction (light grey pixels), the threshold was defined between 160 and 220. The total pixel area of the bone-biomaterial interface selection was defined by the total image pixels, between 0 and 240 (Fig. 2).

3. Statistical analysis

Statistical analysis was performed using GraphPad Prism (version 6.00 for Mac OS X, GraphPad Software, La Jolla California USA). Results were presented as Mean ± Standard Error of the Mean (Mean ± SEM). Comparisons between groups were performed by two-tailed unpaired *t*-test (IC95%). Differences were considered statistically significant when $P \leq 0.05$. Significant results between groups were presented using the symbol (*). Significant results are also indicated according to *P* values with one, two, three or four of the symbols (*) corresponding to $0.01 < P \leq 0.05$, $0.001 < P \leq 0.01$, $0.0001 < P \leq 0.001$ e $P \leq 0.0001$, respectively.

4. Results

4.1. Bonelike® Poro characterization

BLP XRD data set (Fig. 3) confirmed the presence of HA, α-tricalcium phosphate (α-TCP) and β-tricalcium phosphate (β-TCP) in respective proportions of approximately 65%, 30% and 5%. These calculations were based upon the intensity of the main peaks of each phase.

The results regarding SEM analysis are shown in Fig. 4 and as it may be seen in Fig. 4A the structure of BLP is quite homogeneous and composed of large pores and pore interconnectivity. Fig. 4B shows that the granules were well-sintered and, also, some microporosity. The SEM analysis showed macropores with diameters between values ranging from 200 to 600 μm (Fig. 4A) and micropores between values close to 1,5 μm and 550 nm (Fig. 4B) approximately. This image is an example of the entire structure of the material. Macro- and microporosities provide sites for cell adhesion and the interconnectivity between pores is required for the transport of nutrients. These properties favor cell adhesion/proliferation and, consequently, lead to bone tissue growth (Laranjeira et al., 2009; Gutierres et al., 2008).

4.2. In vivo bone regeneration assessment

All animals recovered from the anaesthesia without major complications and remained so throughout the study period. At the defined time point animals were sacrificed and *ilia* were explanted and analysed.

4.2.1. Macroscopic analysis

After soft tissue removal, the defect area was inspected. All the treated defects (BLP and AG groups) presented filling of the defect area with tissue of hard consistency, compatible with satisfactory macroscopic bone healing. The control defects presented a soft consistency due to the failure in ossification and the presence of fibrous tissues.

4.2.2. Radiographic analysis

Qualitative analysis of the *in vivo* postoperative radiographic images confirmed the radiopaque filling of the engineered bone defects, as shown in Fig. 5. The BLP treated group presented a more intense radiopaque signal at the lesion site, indicating greater density of the BL granules, when comparing to the autograft treated group. Regarding *post mortem* evaluation of *ex vivo* radiographic images, new bone formation within the defects was observed in all samples. Control defects presented minimal bone deposition at the limit of the defect and incomplete bone healing, thus confirming the lesion model as a critical bone defect. Defects presented a small grey line in the limit of the defect and a radiolucent circle inside, due to the presence of fibrous tissues. Defects filled with BLP and AG showed evidence of reduced radiolucency, indicating a more effective mineralization process. Between both groups, BLP treated group continued to present a more radiopaque signal at the lesion site, as observed in the immediate postoperative images, thus indicating BLP presence on site after the recovery period of 5 months. It is possible to observe a continuity between the BLP granules and the newly formed bone, as the defect line is less evident when comparing to the AG treated group. Images allowed to infer the BLP granules integration in the new bone matrix. AG treated group presented a more radiolucent defect filling, indicating a less competent matrix formation for the newly-

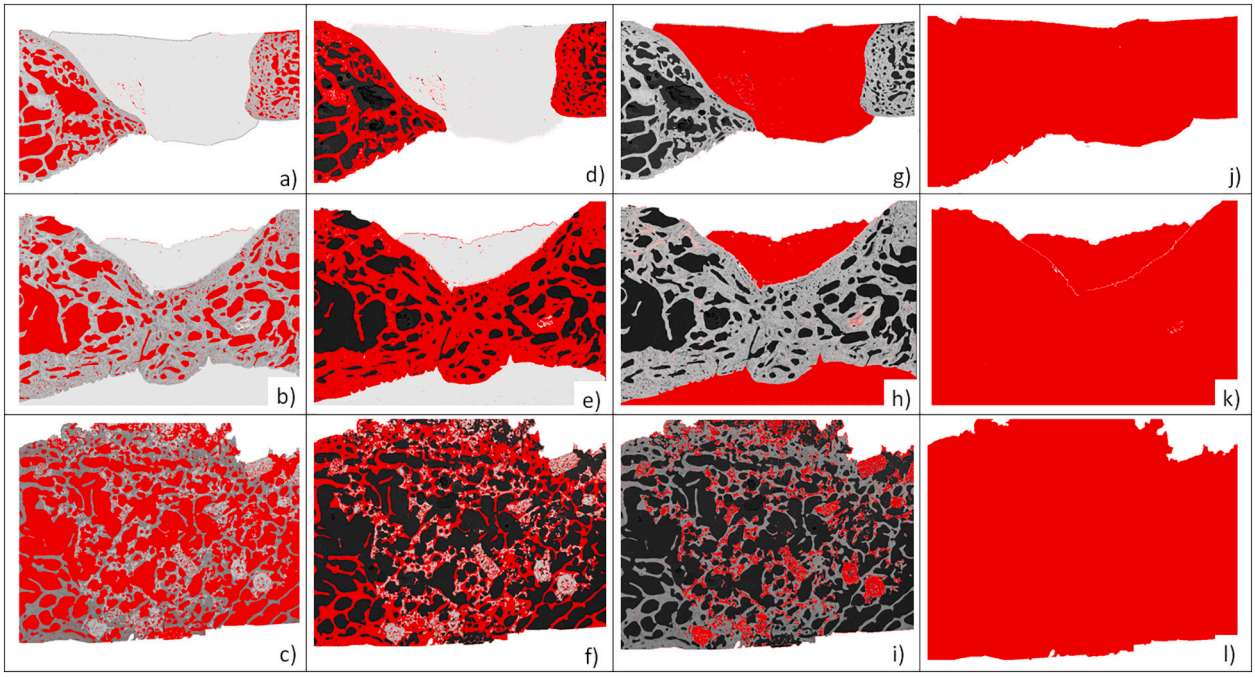

Fig. 2. Image Processing Sequence of the defect area using ImageJ® software and threshold analysis tool. CT group: upper panel, AG group: middle panel, BL group: lower panel. Unmineralized voids: a, b, c; Bone: d, e, f; Unfilled area (connective tissue): g, h; Biomaterial: i; Total area: j, k, l.

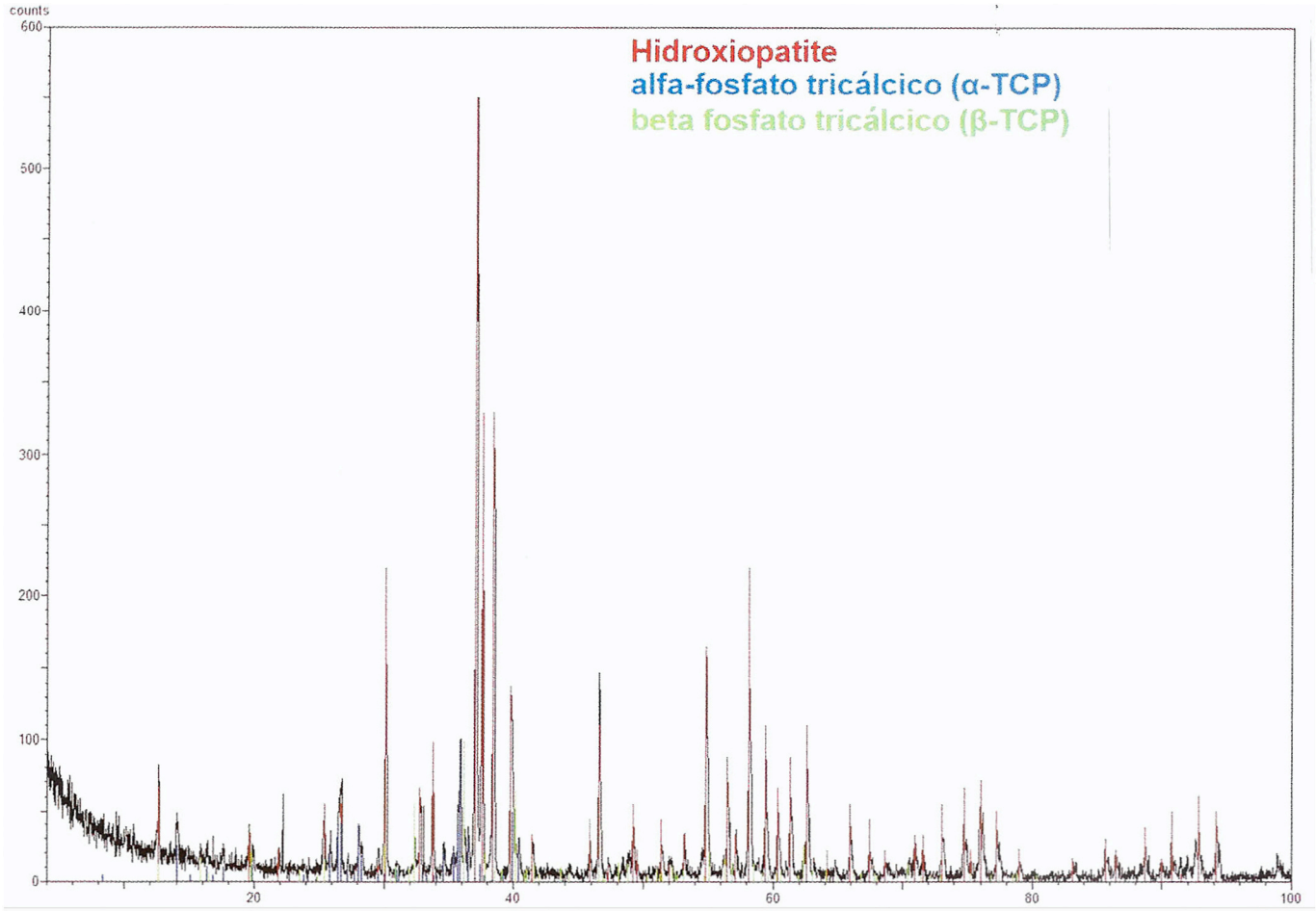

Fig. 3. XRD diffractogram of BMP showing the presence of the 3 crystalline phases, HA, β-TCP and α-TCP.

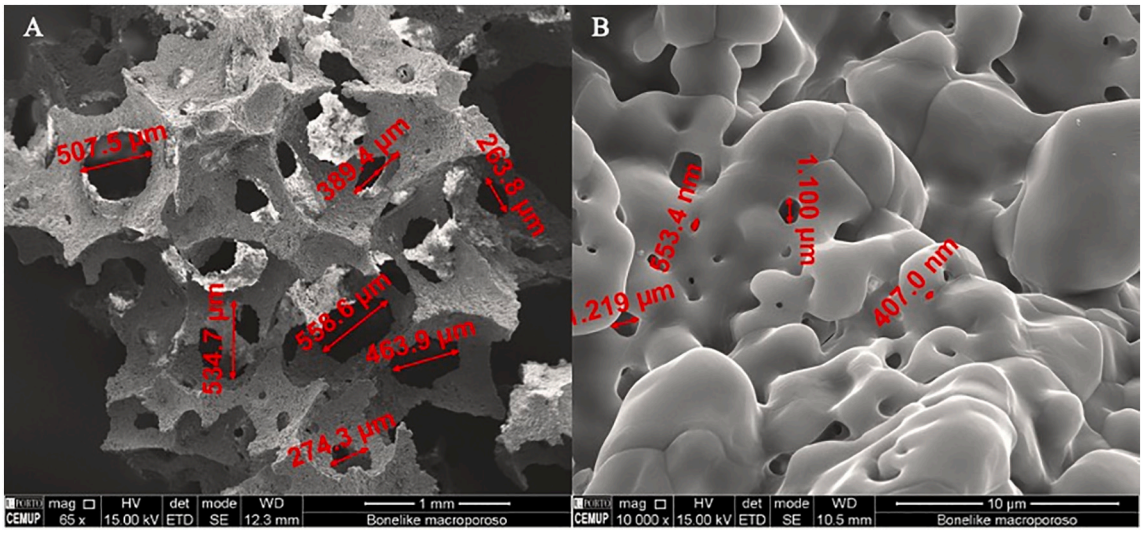

Fig. 4. SEM images of BMP (Total magnification: A - 65×, B -10,000×).

formed bone.

4.2.3. Histological processing and scanning electron microscopy (SEM)

SEM was employed for the bone segments, allowing visualization of the entire defect area, including the surrounding healthy bone segments. Fig. 6 compares histological and SEM images of the defect areas for each group.

EDS analysis was performed, comparing the bone, biomaterial and connective tissue (unfilled area) fractions (Fig. 7). EDS analysis allowed to detect the presence of Calcium, Magnesium, Phosphorus and Sodium in the bone fraction. A similar composition regarding the biomaterial and bone fraction was also observed (lower panel). Amplified SEM

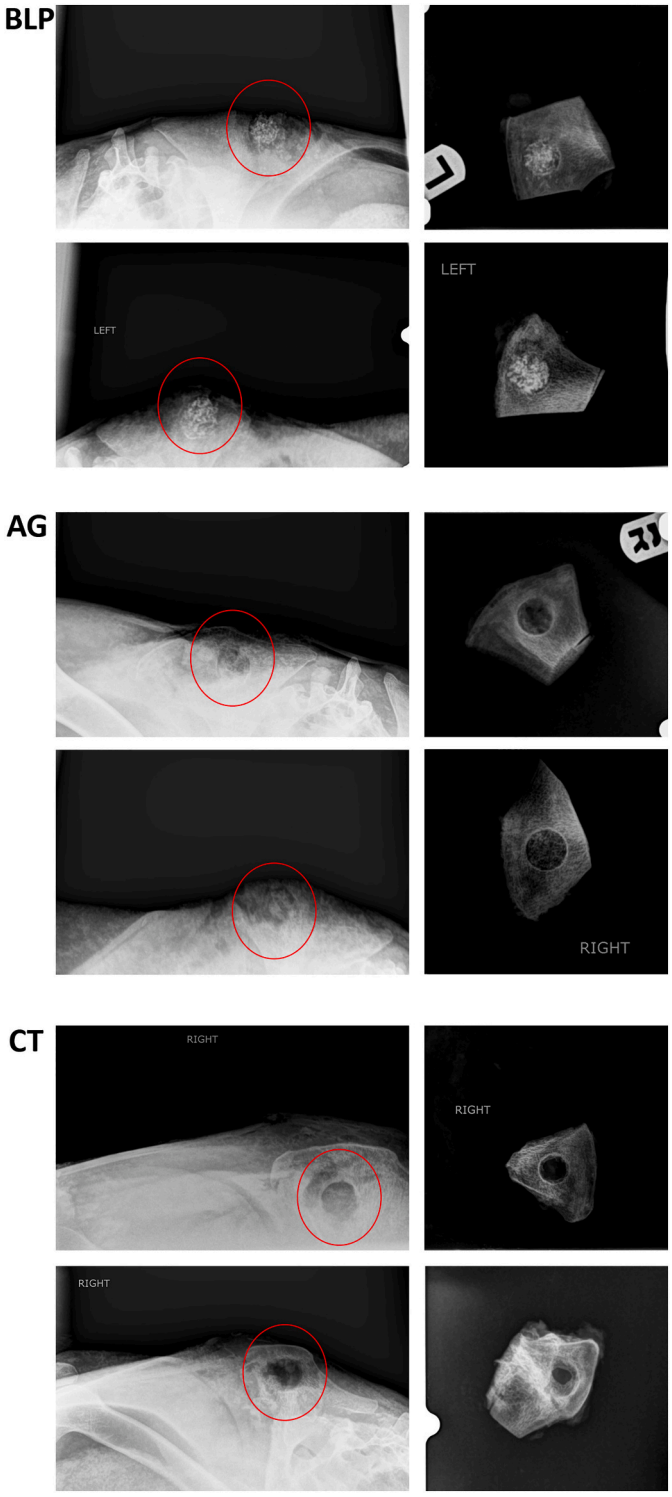

Fig. 5. *In vivo* post-operative (left) and *post-mortem ex vivo* (right) representative X-Ray images for BLP, AG and CT groups. Defects *in vivo* highlighted in red.

images of the bone samples is presented in Fig. 8.

Regarding the histological analysis, based on ISO 10993-6:2016 Annex D (implantation in bone) and Sinikovic et al. score system (Šiniković et al., 2007), bone healing process evaluation was performed using a microscope Eclipse E600 (Nikon®) and the software Imaging Software NIS-Elements F Ver4.30.01 (Laboratory Imaging®). Table 1 presents the score system applied, with slight adaptations regarding the one developed by Sinikovic et al. Histological score results are presented in Table 2. A representative image for each different score classification is represented in Fig. 9.

No major events of inflammation or fibrous tissue deposition were observed surrounding BLP particles. In the AG group, healing indicators presented some noteworthy inter-sample variability, and one sample displayed signs of graft encapsulation and abscess formation, resulting in inferior osseous regeneration.

New bone integrated the lamellar bone of the defect margin and penetrated into the porous structure of the bonelike granules, involving the particles. The newly formed tissue presented healthy bone features, with embedded osteocytes and active osteoblasts adjacent to osteoid seams.

4.2.4. *Histomorphometric analysis*

SEM images were obtained for all samples and were further analysed histomorphometrically, evaluating osteo-integration and osteo-conduction. Regarding the CT group, bone healing was incomplete, as the defect area remained unmineralized, and without the formation of a bone bridge. These results are consistent, as the defect size performed is categorized as a critical defect (bone healing capacity outweighed). The AG group presented samples with complete bone bridge formation, as well as incomplete ones. Regarding the biomaterial-treated group, all samples presented complete bone bridging and good integration of the biomaterials in the bone tissue, with unfilled areas are almost undetectable (Fig. 2). The unmineralized voids, bone, unfilled and biomaterial fractions were quantified and corrected to the total pixel area. Results of corrected area percentages for each group are presented in Fig. 10 and Table 3.

5. Discussion

The effective treatment of non-unions and critical-sized defects remains challenging for orthopedic surgeons and currently employed surgical approaches share no consensus and bare suboptimal outcomes (Calori et al., 2011; Roddy et al., 2018; Toogood and Miclau, 2017). From a tissue engineering perspective, it is herewith proposed the application of a *novel* formulation of Bonelike® as bioactive matrix to support bone regeneration, as opposed to the widespread autologous grafting technique.

Biomaterial characterization confirmed the presence of HA combined with β and α -tricalcium phosphate (TCP) crystalline phases (XRD analysis), thus allowing ideal conditions for the bone substitute to be reabsorbed at a rate close to the formation of new bone (Gutierres et al., 2006). Further, the open and interconnected porosity of the BLP (SEM analysis) was also observed, confirming an important characteristic for cell migration, anchoring and bone tissue ingrowth, as well as being a feature described as highly beneficial to biomaterial revascularization, an essential step for tissue integration and efficient remodeling. The regenerating site revascularization grants nutritional support and metabolic waste removal to the active site and provides a route for endogenous inflammatory and regenerative populations to reach into it, improving overall bone regeneration. The impaired vascularization of the defect site has been described as a limiting factor for large biomaterial implants integration, resulting in inefficient tissue ingrowth, matrix remodeling and necrotic events in the core of the implant.

This projected potential was further validated using an animal model of critical-sized bone defect. The choice of the most appropriate animal model is crucial in the testing of bone substitute biomaterials for the understanding of their osteoconductive, osteointegrative and mechanical properties, and also, their biocompatibility, degradations or resorption, and interactions with host tissues (Hollinger and Kleinschmidt, 1990; Atayde et al., 2014; Li et al., 2015; Pinto et al., 2016). In the present model, the defects were performed in a non-weight bearing bone, which permitted the creation of two defects per animal, reducing the number of animals submitted to the experimental procedure. The model's reproducibility was also confirmed, granting the creation of

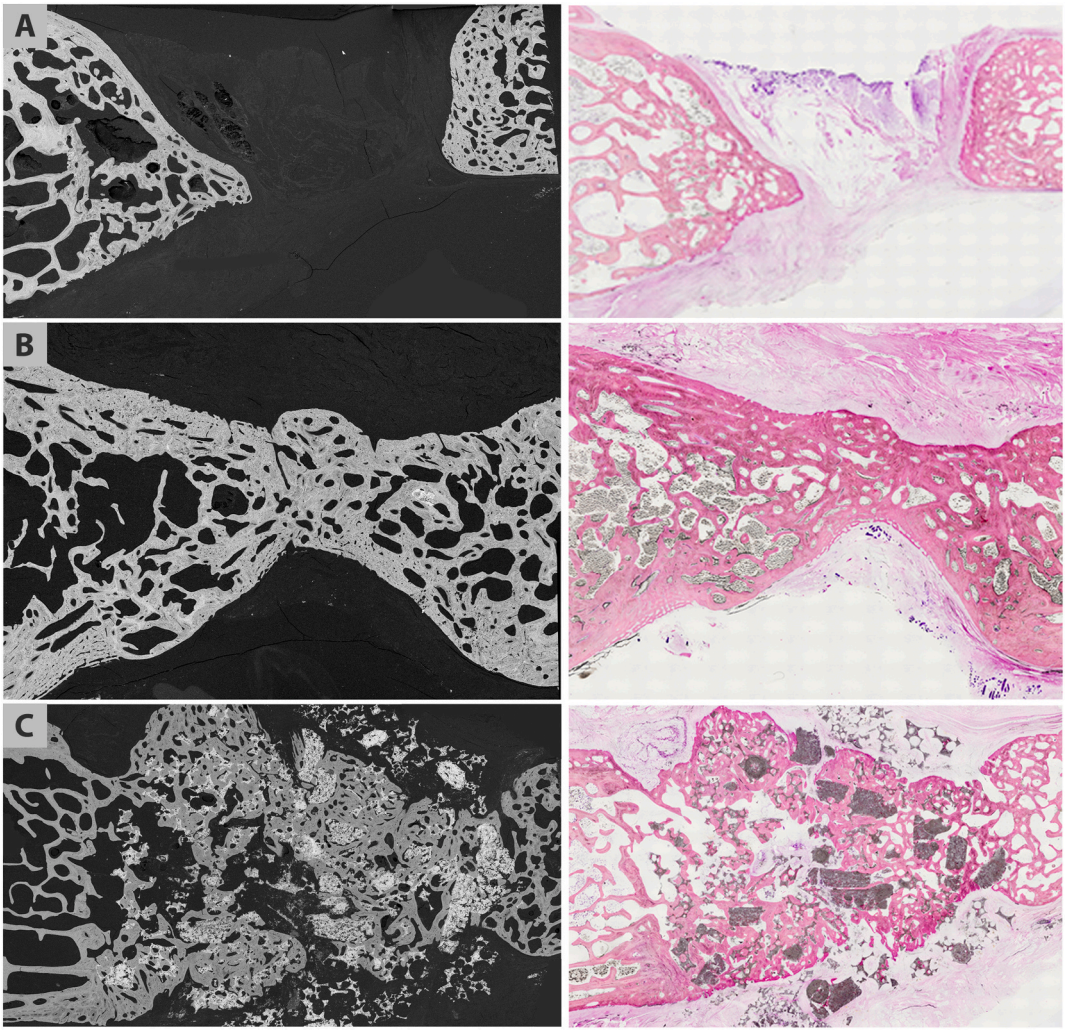

Fig. 6. SEM images (left panel) and corresponding histological images with HE (right panel). A: CT group, B: AG group, C: BLP group.

identical sized defects that presented comparable biological behavior and reducing inter-individual variation, as previously demonstrated by Lansdowne et al. (2014).

After 5 months of recovery, macroscopic observation of the exerted samples suggested good quality of the defect filling tissue in both BLP and AG treated groups, which was further confirmed by microstructural analysis. Efficient bone bridging is evidenced in these groups, while untreated defects failed to heal, developing a non-union with connective tissue formation, confirming the critical nature of the selected defect model (Lansdowne et al., 2014). Radiographic imaging of control defects was characterized by the presence of soft tissue with a grey to black appearance in the center of the lesion, with minimal proliferation of new bone at the edge of the defect, compatible with the presence of fibrous tissue due to lack of bone healing. In both treated groups, the filling tissue appeared harder in nature, with radiopacity similar to that of native bone. Defects filled with BLP granules presented as small radiopaque structures with increased radiopacity due to the high density conferred by the chemical composition of the biomaterial.

In the treated groups, the BLP implantation granted statistically superior bridge thickness and depicted fair integration with the host bone, as assessed through a histological scoring system. The analysis of the core areas of the implant confirmed new bone ingrowth, with characteristic mineral content and histologic features, well imbedded within the biomaterial matrix. The more competent bone bridge formation observed in the BLP treated group, comparing with the AG treated group, indicated a more efficient scaffold function by the synthetic material when compared to natural bone, confirming it to bare increased osteoconductive properties, granted by its chemical composition, porosity, and macroporous architecture (Blokhuis et al., 2000; Gutierres et al., 2008). Porous granules of BLP were demonstrated to support bone ingrowth and remained inside the defect contained by the adjacent muscles and local soft tissues (without periosteum flap or synthetic membrane application). The maintenance of biomaterial within the defect site is a positive observation and bares clinical significance, since material leakage is a major problem is some scenarios, such as calvarial defects (Lansdowne et al., 2014; Cooper et al., 2010) or long bone defects (Roddy et al., 2018; Hahn et al., 2011; Lindsey et al., 2006; Schneiders et al., 2009). In these models or clinical set-ups, the utilization of the osteomimetic materials could be combined with synthetic membranes or Masquelet technique to assist in biomaterial containment (Toogood and Miclau, 2017; Tarchala et al., 2018). However, the lack of synthetic membrane barriers application could be responsible for soft tissue ingrowth, competing for space with newly forming bone, and consequent impaired regeneration potential. Further research is worth towards strategies to overcome the soft tissue invasiveness and deleterious effect on the local bone remodeling, such as the application of collagen-derived barrier membranes, in a guided-bone-regeneration perspective (Barbeck et al., 2020; Stavropoulos et al., 2004). These structures are further reported to have beneficial bioactive and modulating properties (Omar et al., 2019; Sbricoli et al., 2020). Another strategy to consider is the adjuvant use of mesenchymal stem cells, in particular dental pulp stem/stromal cells, presenting significant pro-

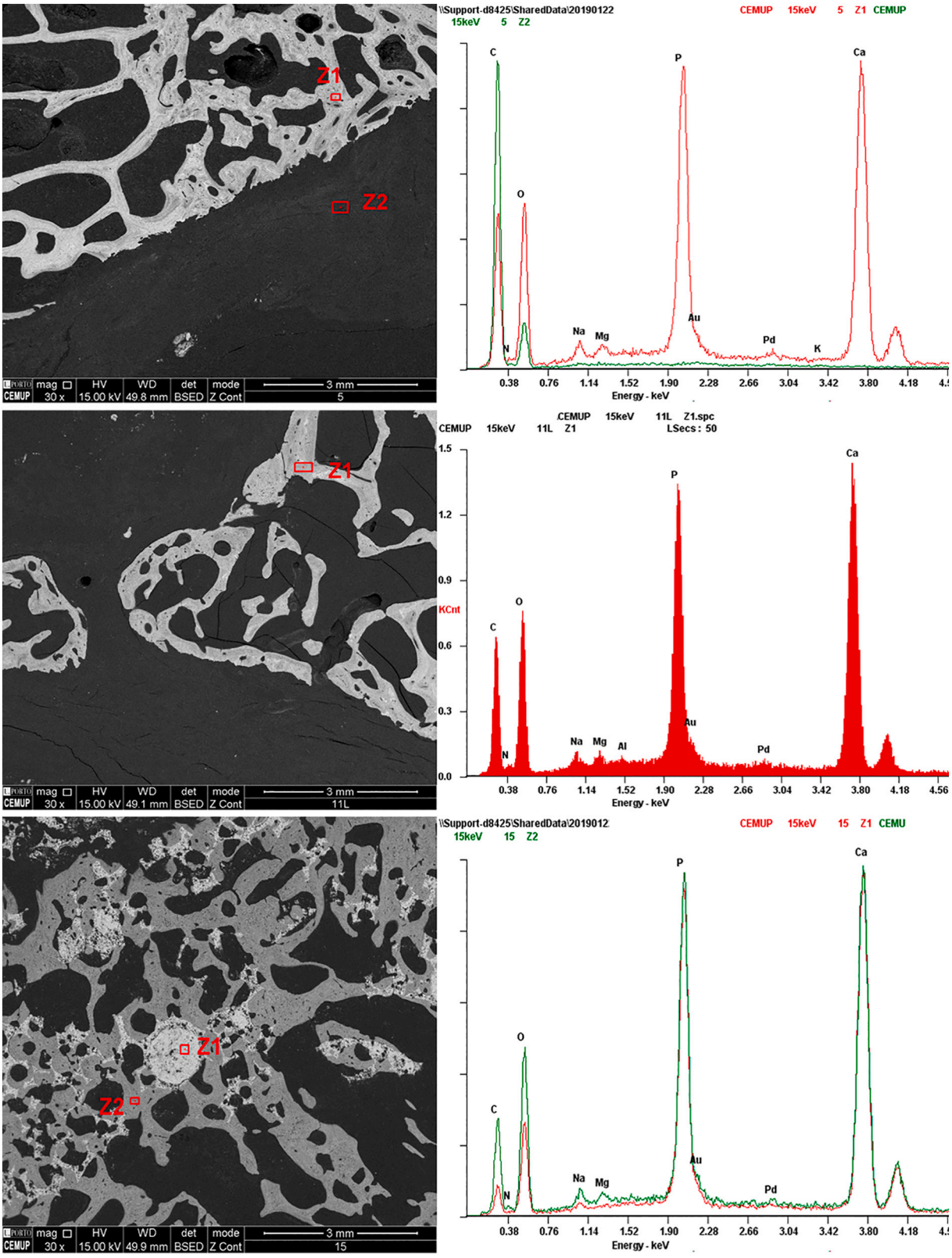

Fig. 7. SEM images and EDS analysis of the bone samples. CT group: upper panel, AG group: middle panel, BLP group: lower panel.

angiogenic and anti-fibrotic properties, thus enhancing the regenerative potential of the applied treatment by introducing osteoinductive properties to the combined therapy (Campos et al., 2018a; Caseiro et al., 2019).

The BLP biocompatibility was validated, with no signs of local or systemic rejection. The higher regenerative indexes were accompanied by tissue maturation and biomaterial granules degradation is also suggested. The presence of healthy bone features (such as the presence of Haversian channels) in close proximity to the bony surface is an indicator of bone deposition and maturation around the graft material. The

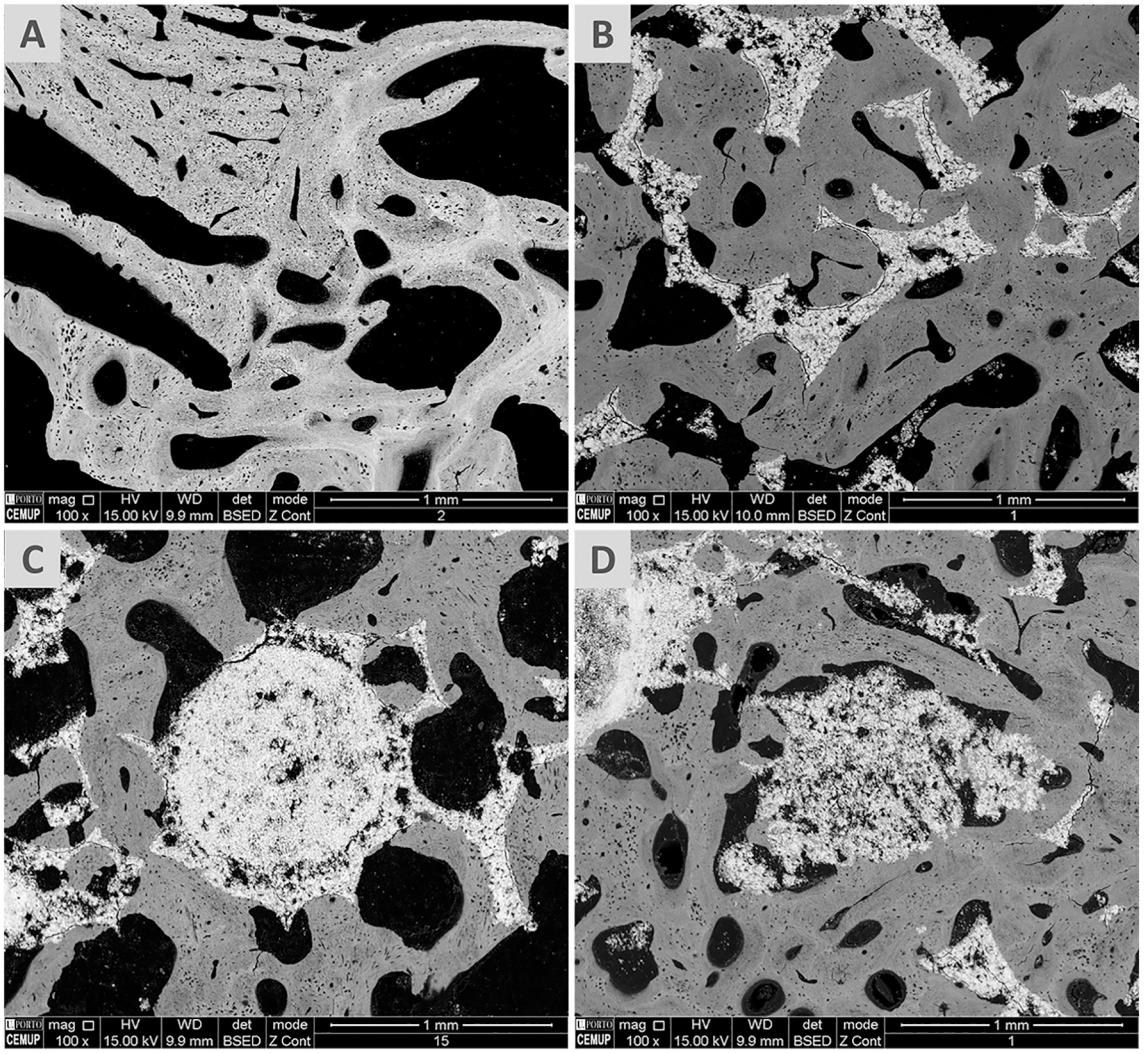

Fig. 8. Amplified SEM images of the bone samples. A: AG group: image detail of the autograft/mature bone interface; B, C and D: BLP group: image detail of Bonelike® interface with newly formed bone.

Table 1
Developed score system for the assessment of biomaterial-host interaction, adapted from Šiniković et al. (2007).

Score	Histological characteristics
5	Bone or osteoid tissue at the edge of the reconstruction material, with continuous transition to the local bone
4.5	Bone or osteoid tissue at the edge of the reconstruction material, with a narrow-like continuity
4	Bone or osteoid tissue at the edge of the reconstruction material, without continuous transition to the local bone
3	No changes at the edge of the reconstruction material
2	Reconstruction material embedded in scar tissue
1	Accumulation of inflammatory cells next to the reconstruction material
0.5	No contact between reconstruction material and local tissue, and severe accumulation of inflammatory cells next to the reconstruction material
0	No contact between reconstruction material and local tissue; no judgment possible

Table 2
Score system application for histological evaluation of bone healing in the ovine model (result presented as mean score).

Score	
Group	Mean
BLP	4.56
AG	3.93
CT	0.00

extensive osteointegration is depicted by the mineral matrix deposition within the granules or directly on their surface, resulting in high quality implant/tissue interface.

One of the AG group samples presented signs of graft site infection, which is indeed one of the limitations assigned to the technique (Lansdowne et al., 2014; Anderson et al., 1999), reinforcing the need to establish safer alternative methodologies and the pertinency of the current study.

The use of Bonelike® as a calcium phosphate-based synthetic bone substitute had been previously demonstrated in non-critical-sized bone defects (Atayde et al., 2015; Cortez et al., 2011; Cortez et al., 2012; Lopes et al., 2001), in its granular formulation (Gutierres et al., 2006; Torres et al., 2014; Atayde et al., 2015; Campos et al., 2018a; Cortez et al., 2011; Cortez et al., 2012; Campos et al., 2018b) or in wedges or cylinders of macroporous architecture (Gutierres et al., 2007; Gutierres et al., 2008), in both human and veterinary application. This report is the first in which the macroporous formulation of Bonelike® was used to fill critical-sized bone defects, resulting in complete bone healing. The observed pattern of osteointegration of Bonelike® was similar in both

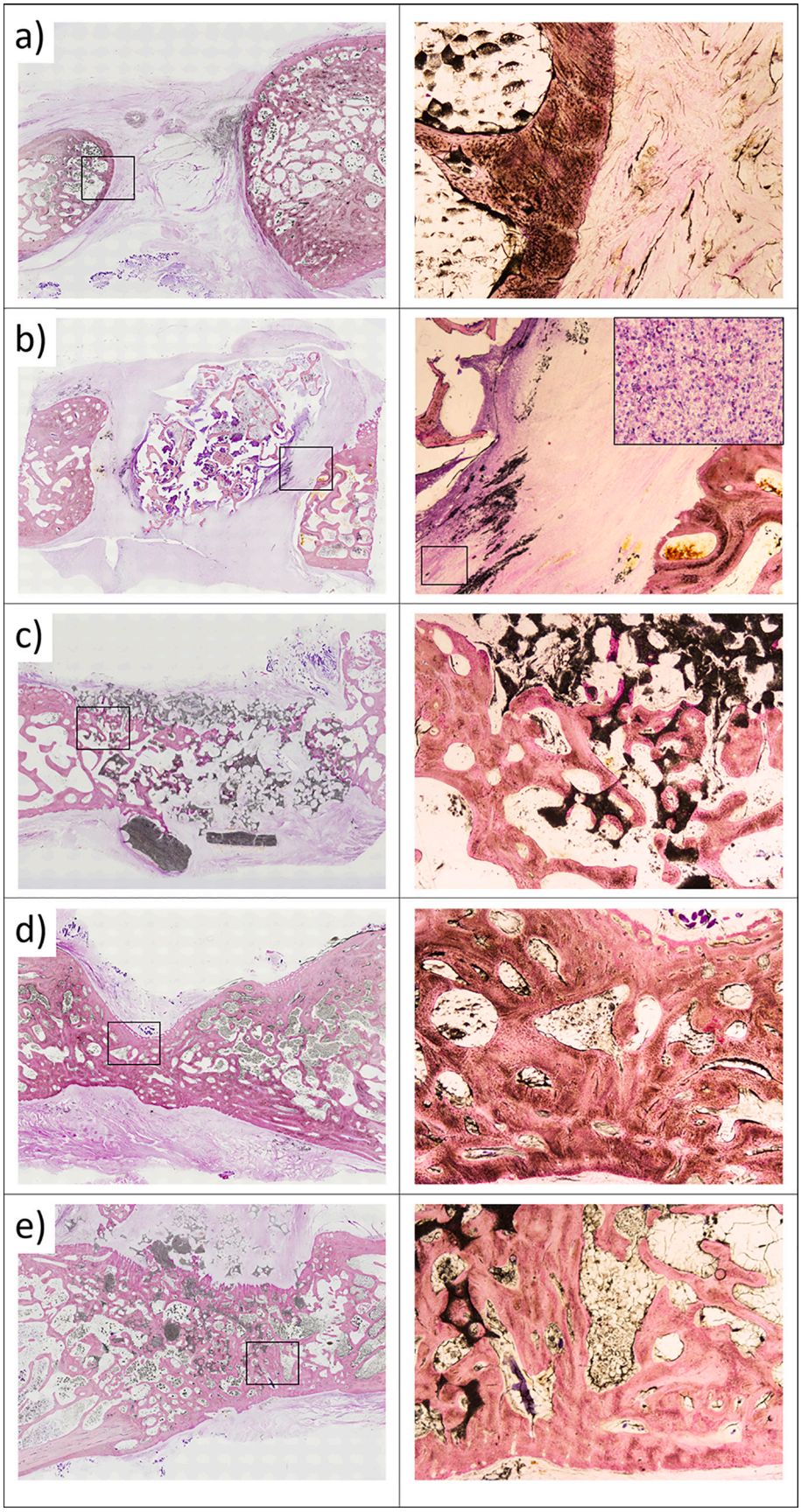

Fig. 9. Histological image stained with H&E. Left panel corresponding to the full scan of the samples and the right panel to a 20× magnification of a specific field of the sample (identified by the insets): a) Score 0 (CT group), b) Score 0,5 (AG group), c) Score 4 (BLP group), d) Score 4,5 (AG group), and e) Score 5 (BLP group).

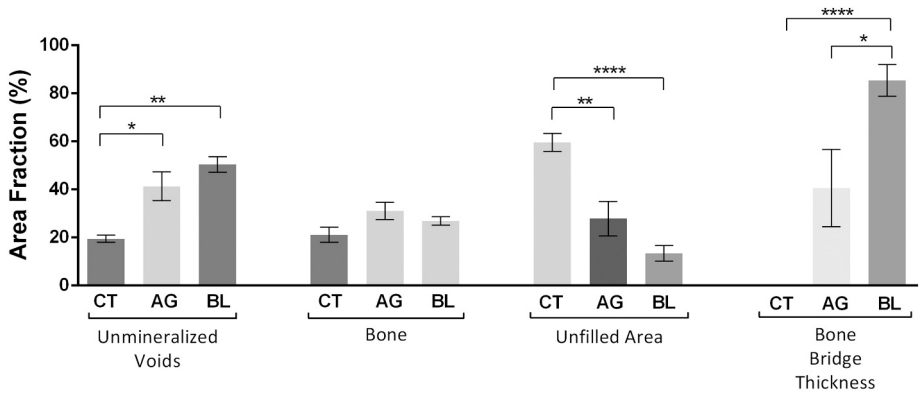

Fig. 10. Area fraction of unmineralized voids, bone, unfilled area (connective tissue) and biomaterial, and bone bridge thickness. Results presented as Mean ± SEM. Significance of the results indicated according to *P* values with one, two, three or four of the symbols (*) corresponding to $0.01 < P \leq 0.05$, $0.001 < P \leq 0.01$, $0.0001 < P \leq 0.001$ e $P \leq 0.0001$, respectively.

Table 3
Area fraction of unmineralized voids, bone, unfilled area (connective tissue) and biomaterial, and bone bridge thickness. Results presented in Mean ± SEM.

Area Fraction (%) of	5 Months								
	CT			AG			BL		
Unfilled	59.48	±	3.78	27.76	±	7.11	13.30	±	3.29
Unmineralized Voids	19.41	±	1.56	41.23	±	6.05	50.38	±	3.28
Bone	21.07	±	3.22	31.01	±	3.61	26.78	±	1.75
Bonelike	0.00	±	0.00	0.00	±	0.00	8.62	±	0.94
Bone Bridge Thickness	0.00	±	0.00	34.72	±	14.81	85.32	±	6.63

situations (Gutierres et al., 2006).

Nevertheless, some limitations can be identified, and are worth addressing in future studies, as the animal model represents only non-weight bearing bones, mimicking a mechanical environment different from the observed in long bone lesions, and limiting the direct extrapolation of the observed results (Lansdowne et al., 2014). Also, and although the *os ilium* consists of cortical and cancellous bone similar to that of the metaphysical region of long bones, it differs from long segmental bone defects which consists mainly of cortical bone.

6. Conclusion

This preliminary study focused on the assessment of the performance of BLP as a synthetic bone substitute for the management of CSBD, as alternative to the gold standard bone graft techniques, focusing on the osteoconductive and osteointegrative properties of this biomaterial. The application of Bonelike® Poro enabled the regeneration of critical-sized bone lesions and resulted in comparable bone regeneration performances when compared to the autograph technique, validating its potential for clinical application as a therapeutic strategy for bone regeneration in human and veterinary orthepaedics.

CRediT authorship contribution statement

P.O. Pinto: Investigation, Formal analysis. **M.V. Branquinho:** Investigation, Writing – original draft, Writing – review & editing, Visualization, Formal analysis, Software. **A.R. Caseiro:** Investigation. **A. C. Sousa:** Investigation, Formal analysis, Writing – review & editing. **A. Brandão:** Investigation, Formal analysis, Writing – review & editing, Resources. **S.S. Pedrosa:** Visualization, Formal analysis. **R.D. Alvites:** Investigation, Writing – original draft, Writing – review & editing, Visualization, Formal analysis. **J.M. Campos:** Investigation, Formal analysis. **F.L. Santos:** Investigation. **J.D. Santos:** Supervision, Writing – review & editing. **C.M. Mendonça:** Investigation. **I. Amorim:** Investigation, Visualization, Formal analysis. **L.M. Atayde:** Supervision, Writing – review & editing, Formal analysis, Data curation, Software, Conceptualization, Methodology. **A.C. Maurício:** Supervision, Writing – review & editing, Formal analysis, Data curation, Project administration, Funding acquisition, Resources, Conceptualization, Methodology.

Declaration of competing interest

The authors declare that they have no known competing financial interests or personal relationships that could have appeared to influence the work reported in this paper.

Acknowledgments

This research was supported by Projects PEst-OE/AGR/UI0211/2011 from FCT, and COMPETE 2020, from ANI – Projetos ID&T Empresas em Copromoção, by the project "insitu.Biomas – Reinvent biomanufacturing systems by using an usability approach for in situ clinic temporary implants fabrication" with the reference POCI-01-0247-FEDER-017771, by the project "Print-on-Organs – Engineering bioinks and processes for direct printing on organs" with the reference POCI-01-0247-FEDER-033877, and by the project "Bone2Move - Development of 'in vivo' experimental techniques and modelling methodologies for the evaluation of 4D scaffolds for bone defect in sheep model: an integrative research approach" with the reference POCI-01-0145-FEDER-031146. Mariana Vieira Branquinho (SFRH/BD/146172/2019), Ana Catarina Sousa (SFRH/BD/146689/2019), and Rui Damásio Alvites (SFRH/BD/116118/2016), acknowledge FCT, for financial support.

References

Alkhraisat, M.H., Rueda, C., Jerez, L.B., Mariño, F.T., Torres, J., Gbureck, U., et al., 2010. Effect of silica gel on the cohesion, properties and biological performance of brushite cement. Acta Biomater. 6 (1), 257–265.

Anderson ML, Dhert WJ, de Bruijn JD, Dalmeijer RA, Leenders H, van Blitterswijk CA, et al. Critical size defect in the goat's os ilium: A model to evaluate bone grafts and substitutes. Clinical Orthopaedics and Related Research®. 1999;364:231–9.

Atayde, L., Cortez, P., Pereira, T., Armada-da-Silva, P., Afonso, A., Lopes, M., et al., 2014. A new sheep model with automatized analysis of biomaterial-induced bone tissue regeneration. J. Mater. Sci. Mater. Med. 25 (8), 1885–1901.
Atayde, L., Cortez, P., Afonso, A., Santos, M., Maurício, A., Santos, J., 2015. Morphology effect of bioglass-reinforced hydroxyapatite (Bonelike®) on osteoregeneration. J. Biomed. Mater. Res. B Appl. Biomater. 103 (2), 292–304.
Barbeck, M., Kühnel, L., Witte, F., Pissarek, J., Precht, C., Xiong, X., et al., 2020. Degradation, bone regeneration and tissue response of an innovative volume stable magnesium-supported GBR/GTR barrier membrane. Int. J. Mol. Sci. 21 (9), 3098.
Berner, A., Reichert, J.C., Muller, M.B., Zellner, J., Pfeifer, C., Dienstknecht, T., et al., 2012. Treatment of long bone defects and non-unions: from research to clinical practice. Cell Tissue Res. 347 (3), 501–519.
Blokhuis, T.J., Termaat, M.F., den Boer, F.C., Patka, P., Bakker, F.C., Henk, J.T.M., 2000. Properties of calcium phosphate ceramics in relation to their in vivo behavior. J. Trauma Acute Care Surg. 48 (1), 179.
Calori, G., Mazza, E., Colombo, M., Ripamonti, C., 2011. The use of bone-graft substitutes in large bone defects: any specific needs? Injury. 42, S56–S63.
Campana, V., Milano, G., Pagano, E., Barba, M., Cicione, C., Salonna, G., et al., 2014. Bone substitutes in orthopaedic surgery: from basic science to clinical practice. J Mater Sci Mater Med. 25 (10), 2445–2461.
Campos, J., Sousa, A., Caseiro, A., Pedrosa, S., Pinto, P., Branquinho, M., et al., 2018a. Dental pulp stem cells and Bonelike® for bone regeneration in ovine model. Regenerative biomaterials. 6 (1), 49–59.
Campos, J.M., Sousa, A.C., Pinto, P.O., Ribeiro, J., França, M.L., Caseiro, A.R., et al., 2018b. Application of Bonelike® as synthetic bone graft in orthopaedic and oral surgery in veterinary clinical cases. Biomaterials research. 22 (1), 1–13.
Carlier, A., van Gastel, N., Geris, L., Carmeliet, G., Van Oosterwyck, H., 2014. Size does matter: an integrative in vivo-in silico approach for the treatment of critical size bone defects. PLoS Comput. Biol. 10 (11), e1003888.
Carson, J.S., Bostrom, M.P., 2007. Synthetic bone scaffolds and fracture repair. Injury. 38 (1), S33–S37.
Caseiro, A.R., Santos Pedrosa, S., Ivanova, G., Vieira Branquinho, M., Almeida, A., Faria, F., et al., 2019. Mesenchymal stem/stromal cells metabolomic and bioactive factors profiles: a comparative analysis on the umbilical cord and dental pulp derived stem/stromal cells secretome. PLoS One 14 (11), e0221378.
Cooper, G.M., Mooney, M.P., Gosain, A.K., Campbell, P.G., Losee, J.E., Huard, J., 2010. Testing the "critical-size" in calvarial bone defects: revisiting the concept of a critical-sized defect (CSD). Plast. Reconstr. Surg. 125 (6), 1685.
Cortez, P., Atayde, L., Silva, M., Armada-da-Silva, P., Fernandes, M., Afonso, A., et al., 2011. Characterization and preliminary in vivo evaluation of a novel modified hydroxyapatite produced by extrusion and spheronization techniques. J. Biomed. Mater. Res. B Appl. Biomater. 99 (1), 170–179.
Cortez, P.P., Silva, M.A., Santos, M., Armada-da-Silva, P., Afonso, A., Lopes, M.A., et al., 2012. A glass-reinforced hydroxyapatite and surgical-grade calcium sulfate for bone regeneration: in vivo biological behavior in a sheep model. J. Biomater. Appl. 27 (2), 201–217.
Cross, A., Tobias, K., Johnston, S., 2012. Fracture biology and biomechanics. Veterinary surgery: small animal. 1, 565–571.
Gómez-Barrena, E., Rosset, P., Lozano, D., Stanovici, J., Ermthaller, C., Gerbhard, F., 2015. Bone fracture healing: cell therapy in delayed unions and nonunions. Bone. 70, 93–101.
Gosain, A.K., Song, L., Yu, P., Mehrara, B.J., Maeda, C.Y., Gold, L.I., et al., 2000. Osteogenesis in cranial defects: reassessment of the concept of critical size and the expression of TGF-beta isoforms. Plast. Reconstr. Surg. 106 (2), 360–371 (discussion 72).
Gutierres M, Sooraj Hussain N, Afonso A, Almeida L, Cabral T, Lopes M, et al., editors. Biological behaviour of bonelike® graft implanted in the tibia of humans. Key Engineering Materials; 2005: Trans Tech Publ.
Gutierres, M., Hussain, N.S., Lopes, M., Afonso, A., Cabral, A., Almeida, L., et al., 2006. Histological and scanning electron microscopy analyses of bone/implant interface using the novel bonelike® synthetic bone graft. J. Orthop. Res. 24 (5), 953–958.
Gutierres, M., Dias, A., Lopes, M., Hussain, N.S., Cabral, A., Almeida, L., et al., 2007. Opening wedge high tibial osteotomy using 3D biomodelling bonelike® macroporous structures: case report. J. Mater. Sci. Mater. Med. 18 (12), 2377–2382.
Gutierres, M., Lopes, M., Hussain, N.S., Lemos, A., Ferreira, J., Afonso, A., et al., 2008. Bone ingrowth in macroporous Bonelike® for orthopaedic applications. Acta Biomater. 4 (2), 370–377.
Hahn, J.A., Witte, T.S., Arens, D., Pearce, A., Pearce, S., 2011. Double-plating of ovine critical sized defects of the tibia: a low morbidity model enabling continuous in vivo monitoring of bone healing. BMC Musculoskelet. Disord. 12 (1), 214.
Hernández, L., Gurruchaga, M., Goni, I., 2009. Injectable acrylic bone cements for vertebroplasty based on a radiopaque hydroxyapatite. Formulation and rheological behaviour. J. Mater. Sci. Mater. Med. 20 (1), 89–97.
Hollinger, J.O., Kleinschmidt, J.C., 1990. The critical size defect as an experimental model to test bone repair materials. The Journal of craniofacial surgery. 1 (1), 60–68.
Innes, J., 2014. Bone grafting in small animal orthopaedic surgery. In Practice. 36 (4), 173–181.
Johnson, A.L., Houlton, J.E., Vannini, R., 2005. AO Principles of Fracture Management in the Dog and Cat: Georg Thieme Verlag.
Lansdowne, J.L., Devine, D., Eberli, U., Emans, P., Welting, T.J., Odekerken, J.C., et al., 2014. Characterization of an ovine bilateral critical sized bone defect iliac wing model to examine treatment modalities based on bone tissue engineering. Biomed. Res. Int. 2014.
Laranjeira, M., Dias, A., Santos, J., Fernandes, M., 2009. In vitro biological characterization of macroporous 3D Bonelike® structures prepared through a 3D machining technique. Mater. Sci. Eng. C 29 (3), 930–935.
Li, Y., Chen, S.-K., Li, L., Qin, L., Wang, X.-L., Lai, Y.-X., 2015. Bone defect animal models for testing efficacy of bone substitute biomaterials. Journal of orthopaedic translation. 3 (3), 95–104.
Lindsey, R.W., Gugala, Z., Milne, E., Sun, M., Gannon, F.H., Latta, L.L., 2006. The efficacy of cylindrical titanium mesh cage for the reconstruction of a critical-size canine segmental femoral diaphyseal defect. J. Orthop. Res. 24 (7), 1438–1453.
Lopes, M., Santos, J., Monteiro, F., Ohtsuki, C., Osaka, A., Kaneko, S., et al., 2001. Push-out testing and histological evaluation of glass reinforced hydroxyapatite composites implanted in the tibia of rabbits. Journal of Biomedical Materials Research: An Official Journal of The Society for Biomaterials, The Japanese Society for Biomaterials, and The Australian Society for Biomaterials and the Korean Society for Biomaterials. 54 (4), 463–469.
Marão, H.F., Peitl, O., Magro, Filho O., 2015. Evaluation of Crystallized Biosilicate in the Reconstruction of Calvarial Defects.
Omar, O., Elgali, I., Dahlin, C., Thomsen, P., 2019. Barrier membranes: more than the barrier effect? J. Clin. Periodontol. 46, 103–123.
Pavan Kumar G, Vijayakumar R, Naga Sowmya B, Nandyala SH, Lopes M, Santos JD, editors. Treatment of a Large Cystic Lesion in Anterior Maxilla Using Glass Reinforced Hydroxyapatite–A Case Report. Solid State Phenomena; 2014: Trans Tech Publ.
Percie du Sert N, Ahluwalia A, Alam S, Avey MT, Baker M, Browne WJ, et al. Reporting animal research: Explanation and elaboration for the ARRIVE guidelines 2.0. PLoS biology. 2020;18(7):e3000411.
Pinto, P., Atayde, L., Campos, J., Caseiro, A., Pereira, T., Mendonça, C., et al., 2016. Therapeutic strategies for bone regeneration: the importance of biomaterials testing in adequate animal models. Adv. Compos. Mater. 275–319.
Roddy, E., DeBaun, M.R., Daoud-Gray, A., Yang, Y.P., Gardner, M.J., 2018. Treatment of critical-sized bone defects: clinical and tissue engineering perspectives. European Journal of Orthopaedic Surgery & Traumatology. 28 (3), 351–362.
Sbricoli, L., Guazzo, R., Annunziata, M., Gobbato, L., Bressan, E., Nastri, L., 2020. Selection of collagen membranes for bone regeneration: a literature review. Materials. 13 (3), 786.
Scheer, J.H., Adolfsson, L.E., 2009. Tricalcium phosphate bone substitute in corrective osteotomy of the distal radius. Injury. 40 (3), 262–267.
Schemitsch, E.H., 2017. Size matters: defining critical in bone defect size! J. Orthop. Trauma 31, S20–S22.
Schneiders, W., Reinstorf, A., Biewener, A., Serra, A., Grass, R., Kinscher, M., et al., 2009. In vivo effects of modification of hydroxyapatite/collagen composites with and without chondroitin sulphate on bone remodeling in the sheep tibia. J. Orthop. Res. 27 (1), 15–21.
Silva, MhPd, Lemos, A.F., Ferreira, JmdF, Santos, J.D., 2003. Mechanical characterisation of porous glass reinforced hydroxyapatite ceramics: Bonelike®. Mater. Res. 6 (3), 321–325.
Šiniković, B., Kramer, F.-J., Swennen, G., Lübbers, H.-T., Dempf, R., 2007. Reconstruction of orbital wall defects with calcium phosphate cement: clinical and histological findings in a sheep model. Int. J. Oral Maxillofac. Surg. 36 (1), 54–61.
Stavropoulos, F., Dahlin, C., Ruskin, J.D., Johansson, C., 2004. A comparative study of barrier membranes as graft protectors in the treatment of localized bone defects: an experimental study in a canine model. Clin. Oral Implants Res. 15 (4), 435–442.
Tarchala, M., Engel, V., Barralet, J., Harvey, E.J., 2018. A pilot study: alternative biomaterials in critical sized bone defect treatment. Injury. 49 (3), 523–531.
Toogood, P., Miclau, T., 2017. Critical-sized bone defects: sequence and planning. J. Orthop. Trauma 31 (Suppl. 5), S23.
Torres, J., Gutierres, M., Lopes, M.A., Santos, J.D., Cabral, A., Pinto, R., et al., 2014. Bone marrow stem cells added to a hydroxyapatite scaffold result in better outcomes after surgical treatment of intertrochanteric hip fractures. Biomed. Res. Int. 2014.
Trejo-Iriarte, C.G., Serrano-Bello, J., Gutiérrez-Escalona, R., Mercado-Marques, C., García-Honduvilla, N., Buján-Varela, J., et al., 2019. Evaluation of bone regeneration in a critical size cortical bone defect in rat mandible using microCT and histological analysis. Arch. Oral Biol. 101, 165–171.
Välimäki, V.-V., Aro, H.T., 2006. Molecular basis for action of bioactive glasses as bone graft substitute. Scand. J. Surg. 95 (2), 95–102.
Vertenten, G., Gasthuys, F., Cornelissen, M., Schacht, E., Vlaminck, L., 2010. Enhancing bone healing and regeneration: present and future perspectives in veterinary orthopaedics. Vet. Comp. Orthop. Traumatol. 23 (03), 153–162.
Wang, W., Yeung, K.W., 2017. Bone grafts and biomaterials substitutes for bone defect repair: a review. Bioactive materials. 2 (4), 224–247.
Zwingenberger, S., Nich, C., Valladares, R.D., Yao, Z., Stiehler, M., Goodman, S.B., 2012. Recommendations and considerations for the use of biologics in orthopedic surgery. BioDrugs. 26 (4), 245–256.